

1 **Mitochondrial impairment activates the Wallerian pathway through depletion of**
2 **NMNAT2 leading to SARM1-dependent axon degeneration**

3

4 Andrea Loreto^{*,1}, Ciaran S. Hill^{1,5}, Victoria L. Hewitt², Giuseppe Orsomando³, Carlo
5 Angeletti³, Jonathan Gilley¹, Cristiano Lucci⁴, Alvaro Sanchez-Martinez²; Alexander J.
6 Whitworth², Laura Conforti⁴, Federico Dajas-Bailador^{*,4}, Michael P. Coleman^{*,1}.

7

8 *Corresponding author - (Lead Contact):

9 Prof Michael Coleman Email: mc469@cam.ac.uk

10 *Corresponding author:

11 Dr Andrea Loreto Email: al850@cam.ac.uk

12 *Corresponding author:

13 Dr Federico Dajas-Bailador Email: f.dajas-bailador@nottingham.ac.uk

14

15

16 ¹ John van Geest Centre for Brain Repair, Department of Clinical Neurosciences,
17 University of Cambridge, Forvie Site, Robinson Way, CB2 0PY, Cambridge, UK

18 ² MRC Mitochondrial Biology Unit, University of Cambridge, Cambridge Biomedical
19 Campus, Hills Road, Cambridge, CB2 0XY, UK

20 ³ Department of Clinical Sciences (DISCO), Section of Biochemistry, Polytechnic
21 University of Marche, Via Ranieri 67, Ancona 60131, Italy

22 ⁴ School of Life Sciences, Medical School, University of Nottingham, NG7 2UH,
23 Nottingham, UK

24 ⁵ Current address: Cancer Institute, University College London, WC1E 6AG, London,
25 UK

26 **ABSTRACT**

27 Wallerian degeneration of physically injured axons involves a well-defined molecular
28 pathway linking loss of axonal survival factor NMNAT2 to activation of pro-
29 degenerative protein SARM1. Manipulating the pathway through these proteins led to
30 the identification of non-axotomy insults causing axon degeneration by a Wallerian-
31 like mechanism, including several involving mitochondrial impairment. Mitochondrial
32 dysfunction is heavily implicated in Parkinson's disease, Charcot-Marie-Tooth
33 disease, hereditary spastic paraplegia and other axonal disorders. However, whether
34 and how mitochondrial impairment activates Wallerian degeneration has remained
35 unclear. Here, we show that disruption of mitochondrial membrane potential leads to
36 axonal NMNAT2 depletion in mouse sympathetic neurons, increasing the substrate-
37 to-product ratio (NMN/NAD) of this NAD-synthesising enzyme, a metabolic fingerprint
38 of Wallerian degeneration. The mechanism appears to involve both impaired NMNAT2
39 synthesis and reduced axonal transport. Expression of WLD^S and *Sarm1* deletion both
40 protect axons after mitochondrial uncoupling. Blocking the pathway also confers
41 neuroprotection and increases the lifespan of flies with *Pink1* loss-of-function
42 mutation, which causes severe mitochondrial defects. These data indicate that
43 mitochondrial impairment replicates all the major steps of Wallerian degeneration,
44 placing it upstream of NMNAT2 loss, with the potential to contribute to axon pathology
45 in mitochondrial disorders.

46 INTRODUCTION

47 Studies of axon degeneration following axotomy (Wallerian degeneration) and of the
48 axon-protective protein WLD^S have led to the discovery of critical endogenous
49 regulators of the mechanisms resulting in axon degeneration (Conforti et al., 2014;
50 Gerdts et al., 2016). The current model predicts that the pathway regulating Wallerian
51 degeneration (Wallerian pathway) is activated by the loss in the axon of the labile
52 nicotinamide mononucleotide adenylyl-transferase 2 (NMNAT2), a nicotinamide
53 adenine dinucleotide (NAD)-synthesising enzyme. Axonal NMNAT2 levels decline
54 within a few hours when its transport and/or synthesis are impaired (Gilley and
55 Coleman, 2010). Downstream of NMNAT2 depletion, the pro-degenerative protein
56 sterile alpha and TIR motif-containing protein 1 (SARM1) executes the degeneration
57 program (Gerdts et al., 2015; Gilley et al., 2015; Loreto et al., 2015; Osterloh et al.,
58 2012). To date, expression of WLD^S/NMNATs (which substitute for endogenous
59 NMNAT2 loss) and SARM1 depletion are the most effective means to block the
60 Wallerian pathway and preserve axons in mammals. There is still debate about how
61 NMNAT2 loss leads to SARM1 activation but the rise in its substrate, NMN, appears
62 to be important (Cohen, 2017; Di Stefano et al., 2015, 2017; Loreto et al., 2015; Zhao
63 et al., 2019) as well as the fall in its product, NAD (Essuman et al., 2017; Gerdts et al.,
64 2015; Sasaki et al., 2016).

65 Most studies on the Wallerian pathway have used a physical injury model, but there is
66 clear evidence that related degenerative mechanisms can be activated by many non-
67 injury stresses (Conforti et al., 2014). However, the vast majority of non-axotomy
68 models were performed when a more comprehensive understanding of the Wallerian
69 pathway was lacking and were mostly identified as being Wallerian-like by targeting
70 just a single step in the pathway (either by expressing of WLD^S/NMNATs or, more

71 recently, by *Sarm1* deletion). Both WLD^s and SARM1 have the potential to influence
72 other cellular mechanisms, such as nuclear NAD synthesis and innate immunity,
73 respectively, so involvement of the Wallerian pathway is best supported by multiple
74 lines of evidence.

75 The link between mitochondria and the Wallerian pathway is particularly intriguing.
76 Mitochondrial dysfunction is a common theme in a wide group of neurodegenerative
77 disorders in which axon degeneration is central, including Parkinson's disease (PD),
78 Charcot-Marie-Tooth disease, hereditary spastic paraplegia and Friedrich's ataxia
79 (Court and Coleman, 2012). We and others have previously shown that mitochondria
80 contribute to the later stages of Wallerian degeneration, where the axotomy itself
81 activates the Wallerian pathway (Barrientos et al., 2011; Loreto et al., 2015). However,
82 mitochondrial depolarisation, caused by the mitochondrial uncoupler Carbonyl
83 cyanide m-chlorophenyl hydrazone (CCCP), also leads to degeneration of uninjured
84 axons (Loreto et al., 2015), which is rescued by *Sarm1* deletion (Summers et al.,
85 2014). Additional studies, both *in vitro* and *in vivo*, link the Wallerian pathway to
86 mitochondrial impairment. *Wld^s* mice are protected against nigrostriatal axon
87 degeneration after intraperitoneal administration of the mitochondrial complex-1
88 inhibitor 1-methyl-4-phenyl-1,2,3,6-tetrahydropyridine (MPTP) (Hasbani and O'Malley,
89 2006). WLD^s also preserves neurites and promotes neuronal survival in primary
90 dopaminergic neurons treated with MPP⁺ (the active metabolite of MPTP) (Antenor-
91 Dorsey and O'Malley, 2012). Finally, NMNATs overexpression and *Sarm1* deletion in
92 sensory neurons delay axon degeneration caused by rotenone, another mitochondrial
93 complex-1 inhibitor, in sensory neurons (Press and Milbrandt, 2008; Summers et al.,
94 2014). Thus, we hypothesised that mitochondrial impairment can also act as an
95 upstream cause, equivalent to physical injury, in initiating the Wallerian pathway.

96 Here we combine multiple lines of evidence to firmly establish a role for the Wallerian
97 pathway in axon degeneration caused by mitochondrial depolarisation in the absence
98 of a physical injury. We also corroborate these findings using an *in vivo* genetic model
99 of mitochondrial dysfunction, reporting a neuroprotective role of regulators of Wallerian
100 degeneration in dopaminergic neuron loss in *Pink1* mutant flies.

101 **RESULTS**

102 **Multiple regulators of the Wallerian pathway rescue axon degeneration caused** 103 **by mitochondrial depolarisation**

104 The mitochondrial uncoupler CCCP is widely used to trigger mitochondrial
105 depolarisation and assess the effects of mitochondrial impairment on cellular viability
106 (Ly et al., 2003). Previous work by us and others demonstrated that sympathetic and
107 sensory primary neurons exposed to CCCP undergo disruption of mitochondrial
108 membrane potential and axon degeneration (Loreto et al., 2015; Summers et al.,
109 2014), providing a good experimental model to study mitochondrial dysfunction
110 leading to axon degeneration.

111 A dose-response experiment in superior cervical ganglion (SCG) neurons confirmed
112 previous observations and allowed us to determine the most appropriate concentration
113 of CCCP to use across the study. 50 μ M CCCP induces full mitochondrial
114 depolarization within minutes after its addition (Loreto et al., 2015) and a dramatic
115 depletion of ATP levels within the first 2 hr (Fig. 1A). Importantly, it consistently
116 promoted neurite degeneration when measured at 24 hr post-application (Fig. 1B-G).
117 We then tested whether this degenerative process could be rescued by regulators of
118 the Wallerian pathway. Consistent with previous studies (Summers et al., 2014), we
119 found that *Sarm1*^{-/-} SCG neurites were strongly protected against CCCP toxicity (Fig.
120 1D,E). WLD^S expression was highly protective too at this concentration (Fig. 1F,G).
121 Our findings demonstrate that the degeneration of axons following mitochondrial
122 depolarisation can be delayed by multiple regulators of the Wallerian pathway.

123 **Mitochondrial depolarisation leads to depletion of axonal NMNAT2**

124 NMNAT2 depletion in axons has been proposed as an initial step that triggers the
125 activation of the Wallerian pathway (Gilley and Coleman, 2010; Gilley et al., 2015;

126 Loreto et al., 2015; Walker et al., 2017). We therefore tested whether CCCP treatment
127 led to NMNAT2 depletion in neurites (which were uninjured until immediately prior to
128 harvesting separately from their cell bodies) and found that levels of this protein in
129 neurites rapidly decline from 2 hr after CCCP addition (Fig. 2A,B). Loss of NMNAT2
130 occurred before any visible morphological damage to neurites (Fig. 2C), also
131 confirmed by the absence of changes to β -actin levels (Fig. 2A). Levels of SCG10,
132 another short-lived protein comigrating with NMNAT2 (Milde et al., 2013) and involved
133 in Wallerian degeneration (Shin et al., 2012) and sporadic ALS (Melamed et al., 2019),
134 declined with a similar timecourse (Fig. 2A,B).

135 We have recently reported that lowering the expression of NMNAT2 increases axonal
136 vulnerability to several stresses (Gilley et al., 2019). To test whether lowering NMNAT2
137 expression impairs the ability to withstand mitochondrial impairment, SCG neurons
138 from mice with around 60% (*Nmnat2^{+gtE}*) and 30% (*Nmnat2^{gtBay/gtE}*) of wild type
139 *Nmnat2* mRNA levels in whole brain (Gilley et al., 2019) were exposed to CCCP. We
140 found a significant acceleration of the degeneration process compared to wild type
141 neurons, with clear morphological damage appearing as early as 4 hr in *Nmnat2^{gtBay/gtE}*
142 neurites (Fig. 2D,E).

143 These data suggest that mitochondrial uncoupling activates the Wallerian pathway at
144 an early step and, together with the protection afforded by WLD^S (Fig. 1F,G), they
145 indicate that axonal NMNAT levels modulate axon survival after mitochondrial
146 depolarisation.

147 **NMNAT2 depletion reflects impairment of both axonal transport and synthesis**

148 We next investigated the cause of NMNAT2 depletion after CCCP treatment. Being a
149 labile protein with a half-life of less than an hour (Milde et al., 2013), any cellular
150 process that impairs its replenishment in axons would lead to a rapid decrease in

151 axonal levels. Two potential mechanisms are a deficiency in axonal transport and/or
152 altered synthesis, both of which are ATP-dependent. The finding that NMNAT2 levels
153 also declined in the cell body/ganglia fraction after 4-8 hr of CCCP addition (Fig. 3A,B)
154 suggests that synthesis of the protein is impaired (although enhanced protein
155 degradation cannot be ruled out). However, the NMNAT2 decrease in the cell body
156 fraction was much less marked than that in neurites (Fig. 2A,B), suggesting that
157 impaired protein synthesis is not the only mechanism contributing to the depletion in
158 the neurites. SCG10 levels in the cell body fraction, instead, did not vary significantly
159 (Fig. 3A,B).

160 We next explored whether CCCP alters NMNAT2 axonal transport. We microinjected
161 GFP-tagged NMNAT2 and followed changes in its axonal transport parameters. We
162 found a significant reduction of the percentage of motile NMNAT2 vesicles at 4 and 8
163 hr after CCCP addition (Fig. 3C,D). This may also explain the slight recovery of
164 NMNAT2 levels in cell bodies at 8 hr after CCCP addition following the decline at 4 hr
165 (Fig. 3A,B), as any NMNAT2 that is synthesised would be less efficiently transported
166 into neurites and would accumulate in cell bodies instead. The overall reduction in
167 axonal transport of NMNAT2 appeared to be a result of a combination of impaired
168 anterograde, retrograde and bidirectional transport, although separately none of the
169 individual parameters reached statistical significance (Fig. 3E).

170 Thus, reduced axonal transport of NMNAT2 and reduced synthesis and/or enhanced
171 degradation combine to reduce axonal NMNAT2 levels after CCCP treatment.

172 **Changes in the NMN/NAD ratio following CCCP administration**

173 We have shown that NMNAT2 depletion leads to accumulation of its substrate, NMN,
174 which we suggest promotes axon degeneration (Di Stefano et al., 2015, 2017; Loreto
175 et al., 2015), as well as to NAD depletion, which also plays an important role (Essuman

176 et al., 2017; Sasaki et al., 2016) (Fig. 4A). Thus, changes in NMN/NAD ratio is an
177 additional indicator of Wallerian pathway activation. We previously reported a marked
178 increase of NMN levels in injured sciatic nerves *in vivo* (Di Stefano et al., 2015, 2017).
179 Sasaki and colleagues recently showed a transient increase in NMN levels in sensory
180 neurons after axotomy also *in vitro* (Sasaki et al., 2016). However, selecting the correct
181 time points is difficult due to the substantial cellular material required for the analysis
182 and the rapid degeneration process which compromises the integrity of the plasma
183 membrane, making any measurement unreliable. We therefore tested whether NMN
184 accumulates and NAD declines following mitochondrial depolarisation in *Sarm1*^{-/-} SCG
185 neurons, where the degeneration process following CCCP administration is strongly
186 delayed (Fig. 1D,E). We looked at 12 hr after CCCP treatment, when wild-type neurites
187 showed the first signs of degeneration (Fig. 2C,D), reasoning that an increase in NMN
188 levels should have already occurred. We found a 2-fold increase in NMN levels and a
189 more modest decrease in NAD levels in neurites resulting in a robust increase in the
190 NMN/NAD ratio (Fig. 4B) (Fig. S1A), consistent with the predicted effects of NMNAT2
191 loss. In contrast, changes in the cell bodies were much more modest (Fig. 4C) (Fig.
192 S1B), consistent with levels of NMNAT2 in the soma being less affected after CCCP
193 administration (Fig. 3A,B) and with the presence of nuclear NMNAT1, which will
194 contribute to NMN and NAD homeostasis in this compartment.

195 Several lines of evidence suggest that NMN accumulation is not simply a marker but
196 is a trigger of axon degeneration. Blocking NMN accumulation with FK866, an inhibitor
197 of the NMN-synthesizing enzyme NAMPT (Fig. 4A), delays Wallerian degeneration.
198 Exogenous administration of NMN restores its accumulation in the presence of FK866,
199 reverting the protection (Di Stefano et al., 2015; Loreto et al., 2015). Also scavenging
200 NMN with expression of bacterial enzyme NMN deamidase, which converts NMN into

201 NaMN (Fig. 4A), results in strong protection of injured axons in mouse primary neurons
202 and *in vivo* in mice and zebrafish (Di Stefano et al., 2015, 2017; Loreto et al., 2015).
203 We therefore tested whether NMN accumulation also promotes axon degeneration
204 after CCCP administration. We first confirmed that the levels of NAMPT were not
205 affected by CCCP treatment (Fig. 5A,B). This is important since NAMPT expression
206 is required for NMN synthesis, which results in the accumulation of NMN in the
207 absence of NMNAT2. We then tested whether blocking NMN synthesis with FK866
208 delays CCCP-induced axon degeneration. As with axon degeneration after axotomy
209 (Di Stefano et al., 2015), FK866 treatment strongly delayed neurite degeneration
210 following CCCP administration. Of note, co-administration of exogenous NMN
211 reverted FK866-induced protection (Fig. 5C,D). In contrast to our previous findings (Di
212 Stefano et al., 2015), some studies reported a protective effect of NMN against
213 axotomy-induced axon degeneration (Sasaki et al., 2006), possibly due to differences
214 in incubation time of NMN before transection. Importantly, we confirmed that NMN had
215 no protective effect on the degeneration process when added together with CCCP
216 (Fig. 5E,F). NMNAT2 depletion still occurred in neurites protected by FK866,
217 consistent with its expected protective action downstream of NMNAT2 loss in this
218 situation (Fig. S2A) (Di Stefano et al., 2015). FK866 conferred full protection also when
219 added up to 8 hr after CCCP addition (when NMNAT2 levels in neurites are already
220 dramatically reduced) and halted the progression of the degeneration when added 12
221 hr after CCCP (when neurites appear already damaged) (Fig. S2B,C). This suggests
222 that activation of the pathway might be reversible, or at least the existence of a time
223 window after mitochondrial dysfunction when it can be prevented, which is important
224 in the context of therapeutic intervention in human diseases.

225 Taken together, these data further support a pro-degenerative role of NMN and are
226 an additional confirmation that CCCP causes axon degeneration through the
227 activation of the Wallerian pathway.

228 ***Highwire* deletion rescues loss of dopaminergic neurons in *Pink1 Drosophila*** 229 **mutants**

230 To validate our findings in an *in vivo* model where mitochondrial dysfunction is caused
231 by a genetic mutation, we employed a *Drosophila* mutant with a loss-of-function
232 mutation in the PD-associated gene *Pink1* (*Pink1^{B9}*). *Pink1* is involved in mitochondrial
233 quality control and mutations in this protein are linked to early-onset recessive PD
234 (Pickrell and Youle, 2015; Valente et al., 2001, 2004). Loss of *Pink1* in flies leads to
235 severe mitochondrial defects resulting in, among other phenotypes, loss of
236 dopaminergic neurons (in the PPL1 cluster), locomotor deficits and reduced lifespan
237 (Clark et al., 2006; Hewitt and Whitworth, 2017; Park et al., 2006; Tain et al., 2009).
238 The Wallerian pathway is evolutionary conserved, with several orthologous genes
239 controlling axon degeneration both in mammals and flies (Freeman, 2014) (Fig. S3).
240 As ubiquitous *dSarm* deletion is lethal in *Drosophila*, we instead opted to assess the
241 effects of *Highwire* mutation on the *Pink1^{B9}* phenotype. *Highwire*, and its mammalian
242 ortholog PHR1, are E3 ubiquitin ligases that target *Drosophila* NMNAT (dNMNAT) and
243 NMNAT2, respectively, for proteasomal degradation and *Highwire*/PHR1 depletion
244 appears to delay axon degeneration after axotomy by increasing levels and/or
245 stabilising dNMNAT/NMNAT2, preventing the activation of the Wallerian pathway at
246 an early step (Babetto et al., 2013; Xiong et al., 2012) (Fig. S3).

247 We first tested whether *Highwire* deficiency (*Hiw^{ΔN}*) could rescue the loss of
248 dopaminergic neurons in the PPL1 cluster (Fig. 6A) in *Pink1^{B9}* flies. As *Highwire*
249 mutants display synaptic overgrowth during development at the neuromuscular

250 junction (Wan et al., 2000), we first confirmed that the number of dopaminergic
251 neurons in the PPL1 cluster did not differ from wild-type flies (Fig. 6B,C). Importantly,
252 *Highwire* deletion rescued the loss of dopaminergic neurons in the PPL1 cluster (Fig.
253 6B,C). *Highwire* deletion also significantly prolonged the lifespan of *Pink1^{B9}* flies (Fig.
254 6D), but was not sufficient to rescue climbing and flying ability (Fig. 6E,F), likely due
255 to the widespread muscle degeneration that is also seen in *Pink1^{B9}* flies (Clark et al.,
256 2006; Tain et al., 2009). Modulation of the Wallerian pathway thus appears to be
257 protective against neurodegeneration caused by non-toxin models of mitochondrial
258 disruption in flies.

259 DISCUSSION

260 The data presented here support an involvement of the Wallerian pathway in disorders
261 involving mitochondrial dysfunction. First, acute mitochondrial depolarisation by CCCP
262 leads to axon degeneration, in the absence of a physical injury, through the same
263 pathway that regulates Wallerian degeneration. It does so by impairing axonal
264 transport and synthesis (or stimulating degradation) of the axonal survival enzyme
265 NMNAT2, leading to substantially reduced levels in neurites which increase the
266 NMN/NAD ratio and trigger SARM1-dependent axon degeneration. In addition,
267 neuroprotection of dopaminergic neurons conferred by *Highwire* deletion in flies
268 carrying mutant Pink1 suggests a wider relevance of the Wallerian pathway to different
269 types of mitochondrial insults *in vivo*.

270 Our previous work and that of others suggest a minor contribution of mitochondria to
271 the late stages of Wallerian degeneration after axon transection (Kitay et al., 2013;
272 Loreto et al., 2015), mainly through the opening of mitochondria permeability transition
273 pore and release of Ca²⁺ into the cytoplasm (Barrientos et al., 2011; Villegas et al.,
274 2014). We now show that mitochondrial dysfunction can impact on the Wallerian
275 pathway in a second way, activating it at an early step upstream of NMNAT2. Crucially,
276 like FK866-protected axons (Loreto et al., 2015), *Sarm1*^{-/-} and *Wld^S* axons can be kept
277 morphologically intact for days despite fully depolarised mitochondria (this study and
278 (Loreto et al., 2015; Summers et al., 2014)). This indicates that WLD^S expression and
279 SARM1 deficiency confer protection downstream of mitochondrial impairment (Fig. 7),
280 rather than directly impacting on mitochondrial health.

281 The relevance of the Wallerian pathway beyond its role after axotomy is now widely
282 accepted and mitochondrial depolarisation can now be added to a growing list of non-
283 axotomy insults causing Wallerian-like degeneration, including toxicity caused by

284 chemotherapy agents, chemicals disruption of the nigrostriatal pathway, protein
285 synthesis inhibition and NGF withdrawal (Conforti et al., 2014). Importantly, most of
286 these studies used either WLD^S expression or *Sarm1* deletion as means to assess the
287 involvement of Wallerian-like degeneration. However, these proteins are likely to have
288 additional, non-Wallerian pathway functions and could thus confer a protective
289 phenotype independently of the Wallerian pathway. For example, WLD^S protection
290 against neuropathy and retinopathy in a streptozotocin-induced mouse model of
291 diabetes is linked to a rescue of pancreatic islets (Zhu et al., 2011), likely through a
292 mechanism that is unrelated to its role in axons. Recent steps forward in the
293 understanding of the molecular mechanisms of axon degeneration revealed a well-
294 defined pathway of axon death, with the identification of crucial mechanistic links
295 between NMNAT2 and SARM1 (Gilley et al., 2015, 2017). The knowledge of a core
296 mechanistic pathway allows multiple stages to be probed when seeking to establish a
297 role for the Wallerian pathway in non-axotomy insults and diseases. Here, we followed
298 this approach focusing on NMNAT2 levels, changes in NMN/NAD ratio and protection
299 conferred by WLD^S expression and *Sarm1* deletion. This is the first demonstration of
300 Wallerian pathway involvement at multiple steps in a non-axotomy axonal stress.

301 A next crucial question is whether the activation of the Wallerian pathway contributes
302 to neurodegenerative disorders caused by mitochondrial dysfunction. CCCP is widely
303 used to impair mitochondrial function and has proven instrumental for understanding
304 the role of mitochondria in a number of physiological and non-physiological cellular
305 processes. However, it remains unclear how much its potent and acute mitochondrial
306 toxicity reflects chronic mitochondrial dysfunction in human pathologies. The strong
307 protection achieved by blocking the Wallerian pathway is remarkable, but the extent
308 of mitochondrial damage in neurodegenerative disorders is likely to be milder. The

309 neuroprotection *in vivo* in *Pink1* mutant flies represents a first indication of the possible
310 wider relevance of the Wallerian pathway to other mitochondrial insults *in vivo*,
311 although the use of alternative means to impair mitochondria could provide further
312 understanding of the mechanisms involved. The protection of neuronal soma in
313 *Pink1^{B9}* flies could be secondary to rescue of axon loss. Conversely, *Drosophila* only
314 has one NMNAT isoform (compared to three in mammals) and so a reduction in
315 dNMNAT levels would likely cause a more profound damage to the whole cell, rather
316 than predominantly affecting axons (as it is the case with the major axonal isoform,
317 NMNAT2, in mammals). Finally, we cannot fully rule out the possibility that other
318 actions of Highwire contribute to these observations.

319 Among a number of neurodegenerative disorders associated with mitochondrial
320 dysfunction, the link between PD and axon loss is particularly important. PD involves
321 preferential loss of substantia nigra pars compacta dopaminergic neurons. These
322 neurons have extremely long and branched axons which are lost early in PD patients
323 (Matsuda et al., 2009; Tagliaferro and Burke, 2016), and, as such, may be more
324 vulnerable to axonal stresses. Wallerian-like degeneration has also been implicated
325 in other PD models, with WLD^S protecting after MPTP and 6-hydroxydopamine
326 administration (Cheng and Burke, 2010; Hasbani and O'Malley, 2006; Sajadi et al.,
327 2004), and with neuroprotection in *Pink1* mutant flies by Highwire deficiency that can
328 now be added to the list. However, more comprehensive studies in genetic and chronic
329 models of PD in mammals will be needed to establish whether the Wallerian pathway
330 plays a causative role in PD pathology or simply increases susceptibility to disease.
331 Interestingly, we also show that lower levels of NMNAT2 make neurites more
332 vulnerable to the consequences of CCCP-induced mitochondrial depolarisation and,
333 as NMNAT2 mRNA levels have been reported to vary hugely in the human population

334 (up to 50-fold differences) (Ali et al., 2016), some individuals might thus be at a much
335 higher risk of mitochondrial disorders.

336 To conclude, we show that acute mitochondrial impairment induced by CCCP leads
337 to NMNAT2 depletion and subsequent activation of the Wallerian pathway (Fig. 7),
338 and that loss of dopaminergic neurons as a result of mitochondrial dysfunction in flies
339 with *Pink1* loss-of-function mutation can be prevented by modulation of the Wallerian
340 pathway by *Highwire* deletion. This study provides mechanistic insights on how
341 mitochondrial dysfunction leads to axon degeneration and identifies the Wallerian
342 pathway as a potential contributor to axon pathology in mitochondrial disorders. It is
343 now important to test the role of the pathway in models that more closely replicate
344 human mitochondrial diseases.

345 **MATERIALS AND METHODS**

346 All studies conformed to the institution's ethical requirements in accordance with the
347 1986 Animals (Scientific Procedures) Act.

348 **Primary neuronal cultures**

349 C57BL/6J or CD1 (referred to as wild-type, Charles River, UK), *Wld^S*, *Nmnat2^{+/+}*,
350 *Nmnat2^{+/gtE}*, *Nmnat2^{gtBay/gtE}* and *Sarm1^{-/-}* mouse SCG explants were dissected from
351 P0-2 pups. Explants were cultured in 35 mm tissue culture dishes pre-coated with
352 poly-L-lysine (20 µg/ml for 1 hr; Sigma) and laminin (20 µg/ml for 1 hr; Sigma) in
353 Dulbecco's Modified Eagle's Medium (DMEM, Gibco) with 1% penicillin/streptomycin,
354 100 ng/ml 7S or 50 ng/ml 2.5S NGF (all Invitrogen) and 2% B27 (Gibco). 4 µM
355 aphidicolin (Merck) was used to reduce proliferation and viability of small numbers of
356 non-neuronal cells. For cultures of dissociated SCG neurons, wild-type SCG explants
357 were incubated in 0.025% trypsin (Sigma) in PBS (without CaCl₂ and MgCl₂) (Sigma)
358 for 30 min followed by incubation with 0.2% collagenase type II (Gibco) in PBS for 20
359 min. Ganglia were then gently dissociated using a pipette. Dissociated neurons were
360 plated in a poly-L-lysine and laminin-coated area of ibidi µ-dishes (Thistle Scientific)
361 for microinjection experiments. Dissociated cultures were maintained as explant
362 cultures except that B27 was replaced with 10% fetal bovine serum (Sigma). Culture
363 media was replenished every 3 days. Neurites were allowed to extend for 7 days
364 before performing the experiments.

365 **Drug treatments**

366 Uncut SCG neurons were treated with CCCP or vehicle (DMSO) just prior to imaging
367 (time 0 hr). Unless specified, FK866 (kind gift of Prof. Armando Genazzani, University
368 of Novara) and NMN (Sigma) were added at the same time as CCCP. The incubation

369 time and the drug concentration used for every experiment are indicated in the figures
370 and/or figure legends.

371 **Acquisition of phase contrast images and quantification of axon degeneration**

372 Phase contrast images were acquired on a DMI8 upright fluorescence microscope
373 (Leica microsystems) coupled to a monochrome digital camera (Hamamatsu C4742-
374 95) or on a Zeiss TIRF microscope coupled to an EMCCD (Photometrics PVCam)
375 camera using Axiovision software (Carl Zeiss Inc.). The objectives used were HCXPL
376 20X/0.40 Corr and Zeiss EC Plan Neofluar 20X/0.5 NA. The axon degeneration index
377 (Sasaki et al., 2009) was determined using an ImageJ plugin (Schneider et al., 2012)
378 (<http://rsb.info.nih.gov/ij/download.html>) which calculates the ratio of fragmented axon
379 area over total axon area after binarization of the pictures and subtraction of the
380 background.

381 **Determination of ATP levels**

382 For measurement of ATP levels, dissociated SCG neurons were plated in 96-well
383 plates at the same density. ATP measurements were performed with the ATPlite
384 Luminescence Assay System (PerkinElmer). Two technical repeats were performed
385 per each condition for every experiment. Data are expressed as % relative to DMSO
386 control.

387 **Western blot**

388 Following treatment with CCCP, SCG ganglia were separated from their neurites with
389 a scalpel. Neurites originating from 15 ganglia were collected per condition, washed
390 in ice-cold PBS containing protease inhibitors (Sigma), and lysed directly in 15 µl 2x
391 Laemmli buffer containing 10% 2-Mercaptoethanol (Sigma). The remaining 15 ganglia
392 were also collected and lysed. For NMNAT2 immunoblots, 14 µl of protein samples
393 were loaded on a 12% SDS polyacrylamide gel. For SCG10 and NAMPT immunoblots,

394 1:15 dilutions of the original samples were loaded on a 12% SDS polyacrylamide gel.
395 Membranes were blocked for 3 hr in 5% milk in TBS (50 mM Trizma base and 150
396 mM NaCl, PH 8.3, both Sigma) plus 0.05% Tween-20 (Sigma) (TBST), incubated
397 overnight with primary antibody in 5% milk in TBST at 4°C and subsequently washed
398 in TBST and incubated for 1 hr at room temperature with HRP-linked secondary
399 antibody (Bio-Rad) in 5% milk in TBST. Membranes were washed, treated with ECL
400 (Enhanced Chemiluminescence detection kit; Thermofisher) and imaged with Uvitec
401 Alliance imaging system. The following primary antibodies were used: mouse anti-
402 NMNAT2 (WH0023057M1 Sigma, 2 µg/ml), mouse anti-NAMPT (clone OMNI 379,
403 Cayman Chemical Company, 1:2000) and rabbit anti-SCG10 (10586-1-AP
404 Proteintech, 1:3000). Mouse anti β-actin was used as a loading control (A5316 Sigma,
405 1:5000). Quantification of band intensity was determined by densitometry using
406 ImageJ.

407 **NMNAT2 axonal transport**

408 Dissociated SCG neurons were microinjected using a Zeiss Axiovert S100 microscope
409 with an Eppendorf FemtoJet microinjector and Eppendorf TransferMan®
410 micromanipulator. Plasmids were diluted in 0.5x PBS (without CaCl₂ and MgCl₂) and
411 filtered using a Spin-X filter (Costar). The mix was injected directly into the nuclei of
412 SCG neurons using Eppendorf Femtotips. Approximately 100 neurons were injected
413 per dish. Injected plasmids were allowed to express for 16 hr before CCCP treatment.
414 Plasmids were injected at the following concentrations: 30 ng/µl NMNAT2-EGFP, 30
415 ng/µl pDsRed2-N1. Time-lapse imaging of axonal transport was performed on an
416 Olympus IX70 imaging system with 100X/1.35 Oil objective. During imaging, cell
417 cultures were maintained at 37°C and 5% CO₂ in an environment chamber. Images

418 were captured at 4 frames per sec for 2 min. Three neurites per condition were imaged
419 in every individual experiment.

420 **Determination of NMN and NAD levels**

421 Following treatment with CCCP, *Sarm1*^{-/-} SCG ganglia were separated from their
422 neurites with a scalpel. Neurites and cell bodies were washed in ice-cold PBS and
423 rapidly frozen in dry ice and stored at -80 °C until processed for measuring NMN and
424 NAD. Briefly, pyridine and adenine nucleotides were extracted by sonication in HClO₄
425 in the presence of cAMP (as internal standard) and subsequently analysed by ion pair
426 C18-HPLC chromatography and by spectrofluorometric HPLC analysis after
427 derivatization with acetophenone (Mori et al., 2014). The levels of NMN and NAD were
428 normalised to protein levels.

429 ***Drosophila* experiments**

430 Newly enclosed flies were collected daily and separated by sex into vials of 20-35 flies
431 for aging and experimental use. Genotypes used are *w*¹¹¹⁸ (wild-type), *Pink1*^{B9}, *Hiw*^{ΔN}
432 and *Hiw*^{ΔN} *Pink1*^{B9}. All flies were maintained at a constant 25°C temperature and
433 humidity, in plastic vials with standard agar/cornmeal/yeast feed. Flies were exposed
434 to a 12 hr light-dark cycle. All experiments were conducted on male flies. For PPL1
435 dopaminergic neuron staining, fly brains were dissected in cold 1x PBS and fixed in
436 4% paraformaldehyde-PBS (Sigma) for 30 min. Samples were washed in 1x PBS with
437 0.3% Triton X-100 (Sigma) and blocked for 1 hr at room temperature in 1x PBS with
438 0.3% Triton X-100 and 1% BSA (Sigma). Brains were incubated in primary antibody
439 for 72 hr. After washing and incubation in a fluorescent secondary antibody solution
440 for 4 hr, samples were mounted between two coverslips in ProLong diamond antifade
441 mountant (ThermoFisher). Confocal images were acquired on a Leica microscopy
442 system and blinded for analysis. Antibodies used were mouse anti-Tyrosine

443 Hydroxylase 1:100 (22941, Immunostar Inc.) and secondary anti-mouse IgG (H+L)
444 Alexa Fluor 488 (A11034, ThermoFisher). Flight assay was performed as previously
445 described (Agrawal and Hasan, 2015). Briefly, flies were anaesthetised on ice for 5
446 min; the flat of a 30G 1" needle (Sigma) was attached to the anterior notum of a fly
447 just posterior to the neck using clear nail varnish, leaving flight muscles unimpeded.
448 Flies were given 15 min to recover. Needles were fixed in place under a video
449 microscope. If required, a gentle mouth-blown puff of air was used to stimulate flight
450 and the flying time was recorded for 30 sec. This was repeated 3 times per fly and the
451 average of time spent in flight was calculated for each condition. For climbing assays,
452 flies were gently transferred to fresh empty polystyrene vials without anaesthesia with
453 a maximum density of 25 flies per vial. Groups of up to 6 vials were inserted into the
454 RING device and after 5 min for the flies to adjust to the environmental change the
455 device was tapped three times to settle flies to the bottom of the vials. 5 sec after the
456 last tap, a picture was taken to assess the height climbed. Maximum height achieved
457 was graded into 5 mm intervals, flies that climbed less than 5 cm were scored zero,
458 and any fly that exceeded 5 cm was awarded the maximum score. This was repeated
459 3 times at 60 sec intervals and an average score given for that vial.

460 **Statistical analysis**

461 Appropriate statistical testing of data was performed using Prism (GraphPad Software,
462 La Jolla, USA). ANOVA with Tukey's, Sidak's or Bonferroni's post hoc correction (as
463 applicable), and log-rank (Mantel-Cox) test were used in this study. The n numbers in
464 each individual experiment and the tests used are described in the figure legends.
465 A p value < 0.05 was considered significant (****, p<0.0001; ***, p<0.001; **, p<0.01;
466 *, p<0.05; NS, non-significant).

467 **AUTHOR CONTRIBUTIONS**

468 A.L., L.C. and M.P.C conceived the study. A.L. designed and conducted most
469 experiments and data analysis. C.S.H., V.L.H., A.S-M., and A.J.W. performed
470 experiments on flies. G.O. and C.A. performed nucleotide measurements and related
471 data analysis. C.L. helped with western blots. F.D.-B and M.P.C supervised and co-
472 ordinated the research. A.L., F.D.-B and M.P.C. wrote the manuscript, with input from
473 J.G..

474

475 **ACKNOWLEDGMENTS**

476 We thank the members of the Coleman, Conforti and Dajas-Bailador lab for useful
477 discussion. We thank Dr Jemeen Sreedharan for advice on fly experiments. This work
478 was funded by the Faculty of Medicine and Health Sciences, School of Life Sciences
479 (University of Nottingham), a Parkinson's UK grant [grant number G-1602], the UK
480 Medical Research Council [grant number MR/N004582/1 and MC_UU_00015/6], a
481 Wellcome Trust PhD Fellowship for Clinicians and a Sir Henry Wellcome postdoctoral
482 fellowship from the Wellcome Trust [grant number 210904/Z/18/Z].

483

484 **COMPETING FINANCIAL INTERESTS STATEMENT**

485 The authors declare no conflict of interest.

486 REFERENCES

487

488 Agrawal, T., and Hasan, G. (2015). Maturation of a central brain flight circuit in
489 *Drosophila* requires Fz2/Ca²⁺ signaling.

490 Ali, Y.O., Allen, H.M., Yu, L., Li-Kroeger, D., Bakhshizadehmahmoudi, D., Hatcher, A.,
491 McCabe, C., Xu, J., Bjorklund, N., Taglialatela, G., et al. (2016). NMNAT2:HSP90
492 Complex Mediates Proteostasis in Proteinopathies. *PLOS Biol.* 14, e1002472.

493 Antenor-Dorsey, J.A.V., and O'Malley, K.L. (2012). WldS but not Nmnat1 protects
494 dopaminergic neurites from MPP⁺ neurotoxicity. *Mol. Neurodegener.* 7, 5.

495 Babetto, E., Beirowski, B., Russler, E., Milbrandt, J., and DiAntonio, A. (2013). The
496 Phr1 ubiquitin ligase promotes injury-induced axon self-destruction. *Cell Rep.* 3,
497 1422–1429.

498 Barrientos, S.A., Martinez, N.W., Yoo, S., Jara, J.S., Zamorano, S., Hetz, C., Twiss,
499 J.L., Alvarez, J., and Court, F.A. (2011). Axonal Degeneration Is Mediated by the
500 Mitochondrial Permeability Transition Pore. *J. Neurosci. Off. J. Soc. Neurosci.* 31,
501 966–978.

502 Cheng, H.-C., and Burke, R.E. (2010). The WldS mutation delays anterograde, but not
503 retrograde, axonal degeneration of the dopaminergic nigro-striatal pathway in vivo. *J.*
504 *Neurochem.* 113, 683–691.

505 Clark, I.E., Dodson, M.W., Jiang, C., Cao, J.H., Huh, J.R., Seol, J.H., Yoo, S.J., Hay,
506 B.A., and Guo, M. (2006). *Drosophila* pink1 is required for mitochondrial function and
507 interacts genetically with parkin. *Nature* 441, 1162.

508 Cohen, M.S. (2017). Axon Degeneration: Too Much NMN Is Actually Bad? *Curr. Biol.*
509 27, R310–R312.

510 Conforti, L., Gilley, J., and Coleman, M.P. (2014). Wallerian degeneration: an
511 emerging axon death pathway linking injury and disease. *Nat. Rev. Neurosci.* 15, 394–
512 409.

513 Court, F.A., and Coleman, M.P. (2012). Mitochondria as a central sensor for axonal
514 degenerative stimuli. *Trends Neurosci.* 35, 364–372.

515 Di Stefano, M., Nascimento-Ferreira, I., Orsomando, G., Mori, V., Gilley, J., Brown, R.,
516 Janeckova, L., Vargas, M.E., Worrell, L.A., Loreto, A., et al. (2015). A rise in NAD
517 precursor nicotinamide mononucleotide (NMN) after injury promotes axon
518 degeneration. *Cell Death Differ.* 22, 731–742.

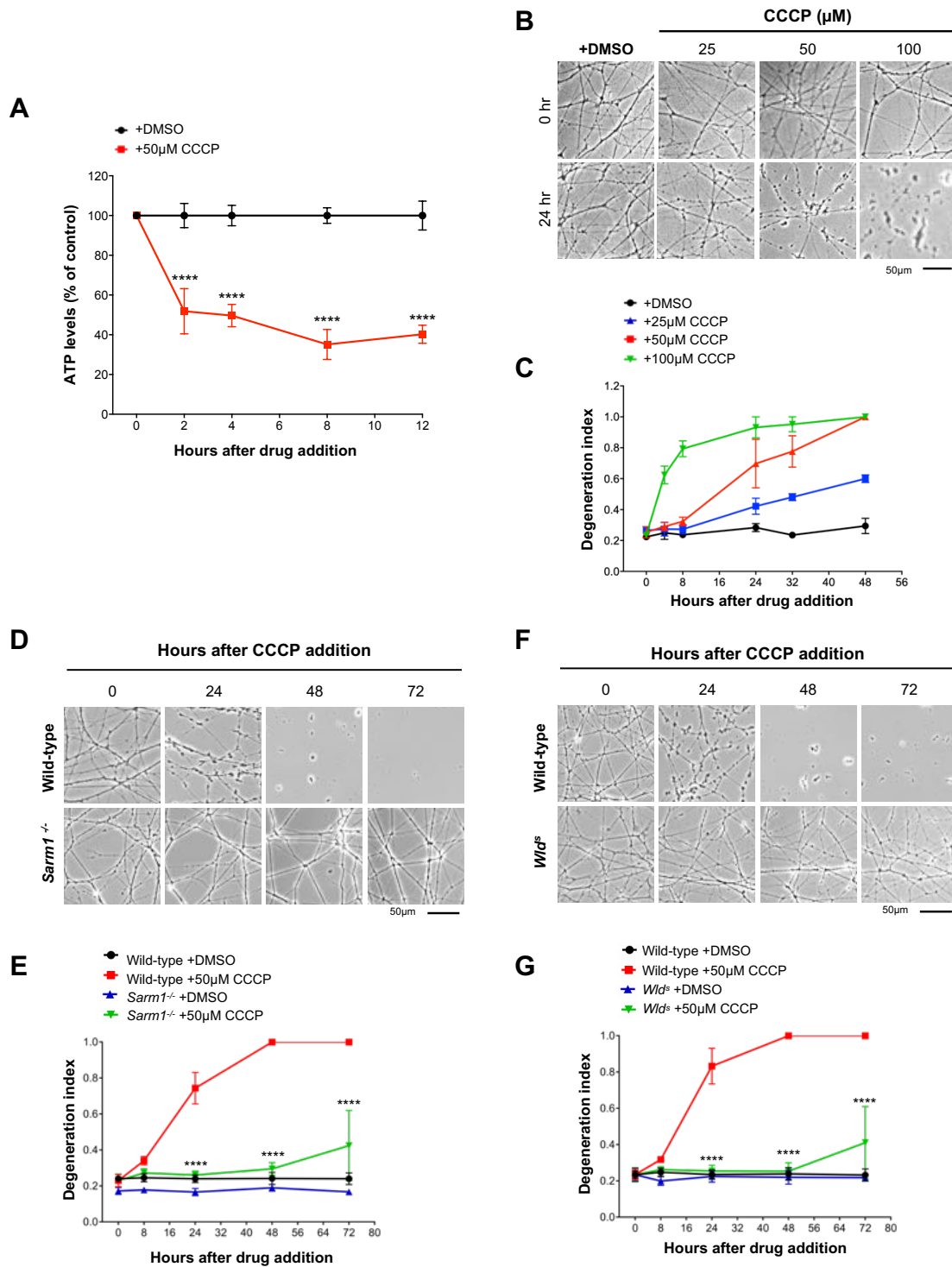
519 Di Stefano, M., Loreto, A., Orsomando, G., Mori, V., Zamporlini, F., Hulse, R.P.,
520 Webster, J., Donaldson, L.F., Gering, M., Raffaelli, N., et al. (2017). NMN Deamidase
521 Delays Wallerian Degeneration and Rescues Axonal Defects Caused by NMNAT2
522 Deficiency In Vivo. *Curr. Biol.* 27, 784–794.

523 Essuman, K., Summers, D.W., Sasaki, Y., Mao, X., DiAntonio, A., and Milbrandt, J.
524 (2017). The SARM1 Toll/Interleukin-1 Receptor Domain Possesses Intrinsic NAD⁺

- 525 Cleavage Activity that Promotes Pathological Axonal Degeneration. *Neuron* 93, 1334-
526 1343.e5.
- 527 Freeman, M.R. (2014). Signaling mechanisms regulating Wallerian degeneration.
528 *Curr. Opin. Neurobiol.* 0, 224–231.
- 529 Gerdts, J., Brace, E.J., Sasaki, Y., DiAntonio, A., and Milbrandt, J. (2015). SARM1
530 activation triggers axon degeneration locally via NAD⁺ destruction. *Science* 348, 453–
531 457.
- 532 Gerdts, J., Summers, D.W., Milbrandt, J., and DiAntonio, A. (2016). Axon Self-
533 Destruction: New Links among SARM1, MAPKs, and NAD⁺ Metabolism. *Neuron* 89,
534 449–460.
- 535 Gilley, J., and Coleman, M.P. (2010). Endogenous Nmnat2 Is an Essential Survival
536 Factor for Maintenance of Healthy Axons. *PLOS Biol.* 8, e1000300.
- 537 Gilley, J., Orsomando, G., Nascimento-Ferreira, I., and Coleman, M.P. (2015).
538 Absence of SARM1 Rescues Development and Survival of NMNAT2-Deficient Axons.
539 *Cell Rep.* 10, 1974–1981.
- 540 Gilley, J., Ribchester, R.R., and Coleman, M.P. (2017). Sarm1 Deletion, but Not WldS,
541 Confers Lifelong Rescue in a Mouse Model of Severe Axonopathy. *Cell Rep.* 21, 10–
542 16.
- 543 Gilley, J., Mayer, P.R., Yu, G., and Coleman, M.P. (2019). Low levels of NMNAT2
544 compromise axon development and survival. *Hum. Mol. Genet.* 28, 448–458.
- 545 Hasbani, D.M., and O'Malley, K.L. (2006). WldS mice are protected against the
546 Parkinsonian mimetic MPTP. *Exp. Neurol.* 202, 93–99.
- 547 Hewitt, V.L., and Whitworth, A.J. (2017). Chapter Five - Mechanisms of Parkinson's
548 Disease: Lessons from Drosophila. In *Current Topics in Developmental Biology*, L.
549 Pick, ed. (Academic Press), pp. 173–200.
- 550 Kitay, B.M., McCormack, R., Wang, Y., Tsoulfas, P., and Zhai, R.G. (2013).
551 Mislocalization of neuronal mitochondria reveals regulation of Wallerian degeneration
552 and NMNAT/WLDS-mediated axon protection independent of axonal mitochondria.
553 *Hum. Mol. Genet.* 22, 1601–1614.
- 554 Loreto, A., Di Stefano, M., Gering, M., and Conforti, L. (2015). Wallerian Degeneration
555 Is Executed by an NMN-SARM1-Dependent Late Ca²⁺ Influx but Only Modestly
556 Influenced by Mitochondria. *Cell Rep.* 13, 2539–2552.
- 557 Ly, J.D., Grubb, D.R., and Lawen, A. (2003). The mitochondrial membrane potential
558 ($\Delta\psi_m$) in apoptosis; an update. *Apoptosis* 8, 115–128.
- 559 Matsuda, W., Furuta, T., Nakamura, K.C., Hioki, H., Fujiyama, F., Arai, R., and
560 Kaneko, T. (2009). Single Nigrostriatal Dopaminergic Neurons Form Widely Spread
561 and Highly Dense Axonal Arborizations in the Neostriatum. *J. Neurosci.* 29, 444–453.

- 562 Melamed, Z., López-Erauskin, J., Baughn, M.W., Zhang, O., Drenner, K., Sun, Y.,
563 Freyermuth, F., McMahon, M.A., Beccari, M.S., Artates, J.W., et al. (2019). Premature
564 polyadenylation-mediated loss of stathmin-2 is a hallmark of TDP-43-dependent
565 neurodegeneration. *Nat. Neurosci.* 22, 180.
- 566 Milde, S., Gilley, J., and Coleman, M.P. (2013). Subcellular Localization Determines
567 the Stability and Axon Protective Capacity of Axon Survival Factor Nmnat2. *PLOS*
568 *Biol.* 11, e1001539.
- 569 Mori, V., Amici, A., Mazzola, F., Stefano, M.D., Conforti, L., Magni, G., Ruggieri, S.,
570 Raffaelli, N., and Orsomando, G. (2014). Metabolic Profiling of Alternative NAD
571 Biosynthetic Routes in Mouse Tissues. *PLOS ONE* 9, e113939.
- 572 Osterloh, J.M., Yang, J., Rooney, T.M., Fox, A.N., Adalbert, R., Powell, E.H., Sheehan,
573 A.E., Avery, M.A., Hackett, R., Logan, M.A., et al. (2012). dSarm/Sarm1 is required for
574 activation of an injury-induced axon death pathway. *Science* 337, 481–484.
- 575 Park, J., Lee, S.B., Lee, S., Kim, Y., Song, S., Kim, S., Bae, E., Kim, J., Shong, M.,
576 Kim, J.-M., et al. (2006). Mitochondrial dysfunction in *Drosophila* PINK1 mutants is
577 complemented by parkin. *Nature* 441, 1157–1161.
- 578 Pickrell, A.M., and Youle, R.J. (2015). The Roles of PINK1, Parkin and Mitochondrial
579 Fidelity in Parkinson’s Disease. *Neuron* 85, 257–273.
- 580 Press, C., and Milbrandt, J. (2008). Nmnat delays axonal degeneration caused by
581 mitochondrial and oxidative stress. *J. Neurosci. Off. J. Soc. Neurosci.* 28, 4861–4871.
- 582 Sajadi, A., Schneider, B.L., and Aebischer, P. (2004). Wlds-Mediated Protection of
583 Dopaminergic Fibers in an Animal Model of Parkinson Disease. *Curr. Biol.* 14, 326–
584 330.
- 585 Sasaki, Y., Araki, T., and Milbrandt, J. (2006). Stimulation of Nicotinamide Adenine
586 Dinucleotide Biosynthetic Pathways Delays Axonal Degeneration after Axotomy. *J.*
587 *Neurosci.* 26, 8484–8491.
- 588 Sasaki, Y., Vohra, B.P.S., Lund, F.E., and Milbrandt, J. (2009). Nicotinamide
589 Mononucleotide Adenylyl Transferase-Mediated Axonal Protection Requires
590 Enzymatic Activity But Not Increased Levels of Neuronal Nicotinamide Adenine
591 Dinucleotide. *J. Neurosci. Off. J. Soc. Neurosci.* 29, 5525–5535.
- 592 Sasaki, Y., Nakagawa, T., Mao, X., DiAntonio, A., and Milbrandt, J. (2016). NMNAT1
593 inhibits axon degeneration via blockade of SARM1-mediated NAD⁺ depletion.
- 594 Shin, J.E., Miller, B.R., Babetto, E., Cho, Y., Sasaki, Y., Qayum, S., Russler, E.V.,
595 Cavalli, V., Milbrandt, J., and DiAntonio, A. (2012). SCG10 is a JNK target in the
596 axonal degeneration pathway. *Proc. Natl. Acad. Sci. U. S. A.* 109, E3696–E3705.
- 597 Summers, D.W., DiAntonio, A., and Milbrandt, J. (2014). Mitochondrial Dysfunction
598 Induces Sarm1-Dependent Cell Death in Sensory Neurons. *J. Neurosci.* 34, 9338–
599 9350.

- 600 Tagliaferro, P., and Burke, R.E. (2016). Retrograde Axonal Degeneration in Parkinson
601 Disease. *J. Park. Dis.* 6, 1–15.
- 602 Tain, L.S., Mortiboys, H., Tao, R.N., Ziviani, E., Bandmann, O., and Whitworth, A.J.
603 (2009). Rapamycin activation of 4E-BP prevents parkinsonian dopaminergic neuron
604 loss. *Nat. Neurosci.* 12, 1129–1135.
- 605 Valente, E.M., Bentivoglio, A.R., Dixon, P.H., Ferraris, A., Ialongo, T., Frontali, M.,
606 Albanese, A., and Wood, N.W. (2001). Localization of a Novel Locus for
607 Autosomal Recessive Early-Onset Parkinsonism, PARK6, on Human Chromosome
608 1p35-p36. *Am. J. Hum. Genet.* 68, 895–900.
- 609 Valente, E.M., Abou-Sleiman, P.M., Caputo, V., Muqit, M.M.K., Harvey, K., Gispert,
610 S., Ali, Z., Turco, D.D., Bentivoglio, A.R., Healy, D.G., et al. (2004). Hereditary Early-
611 Onset Parkinson's Disease Caused by Mutations in PINK1. *Science* 304, 1158–1160.
- 612 Villegas, R., Martinez, N.W., Lillo, J., Pihan, P., Hernandez, D., Twiss, J.L., and Court,
613 F.A. (2014). Calcium Release from Intra-Axonal Endoplasmic Reticulum Leads to
614 Axon Degeneration through Mitochondrial Dysfunction. *J. Neurosci.* 34, 7179–7189.
- 615 Walker, L.J., Summers, D.W., Sasaki, Y., Brace, E.J., Milbrandt, J., and DiAntonio, A.
616 (2017). MAPK signaling promotes axonal degeneration by speeding the turnover of
617 the axonal maintenance factor NMNAT2.
- 618 Wan, H.I., DiAntonio, A., Fetter, R.D., Bergstrom, K., Strauss, R., and Goodman, C.S.
619 (2000). Highwire Regulates Synaptic Growth in *Drosophila*. *Neuron* 26, 313–329.
- 620 Xiong, X., Hao, Y., Sun, K., Li, J., Li, X., Mishra, B., Soppina, P., Wu, C., Hume, R.I.,
621 and Collins, C.A. (2012). The Highwire Ubiquitin Ligase Promotes Axonal
622 Degeneration by Tuning Levels of Nmnat Protein. *PLOS Biol.* 10, e1001440.
- 623 Zhao, Z.Y., Xie, X.J., Li, W.H., Liu, J., Chen, Z., Zhang, B., Li, T., Li, S.L., Lu, J.G.,
624 Zhang, L., et al. (2019). A Cell-Permeant Mimetic of NMN Activates SARM1 to
625 Produce Cyclic ADP-Ribose and Induce Non-apoptotic Cell Death. *IScience* 15, 452–
626 466.
- 627 Zhu, S.S., Ren, Y., Zhang, M., Cao, J.Q., Yang, Q., Li, X.Y., Bai, H., Jiang, L., Jiang,
628 Q., He, Z.G., et al. (2011). WldS protects against peripheral neuropathy and
629 retinopathy in an experimental model of diabetes in mice. *Diabetologia* 54, 2440.
- 630



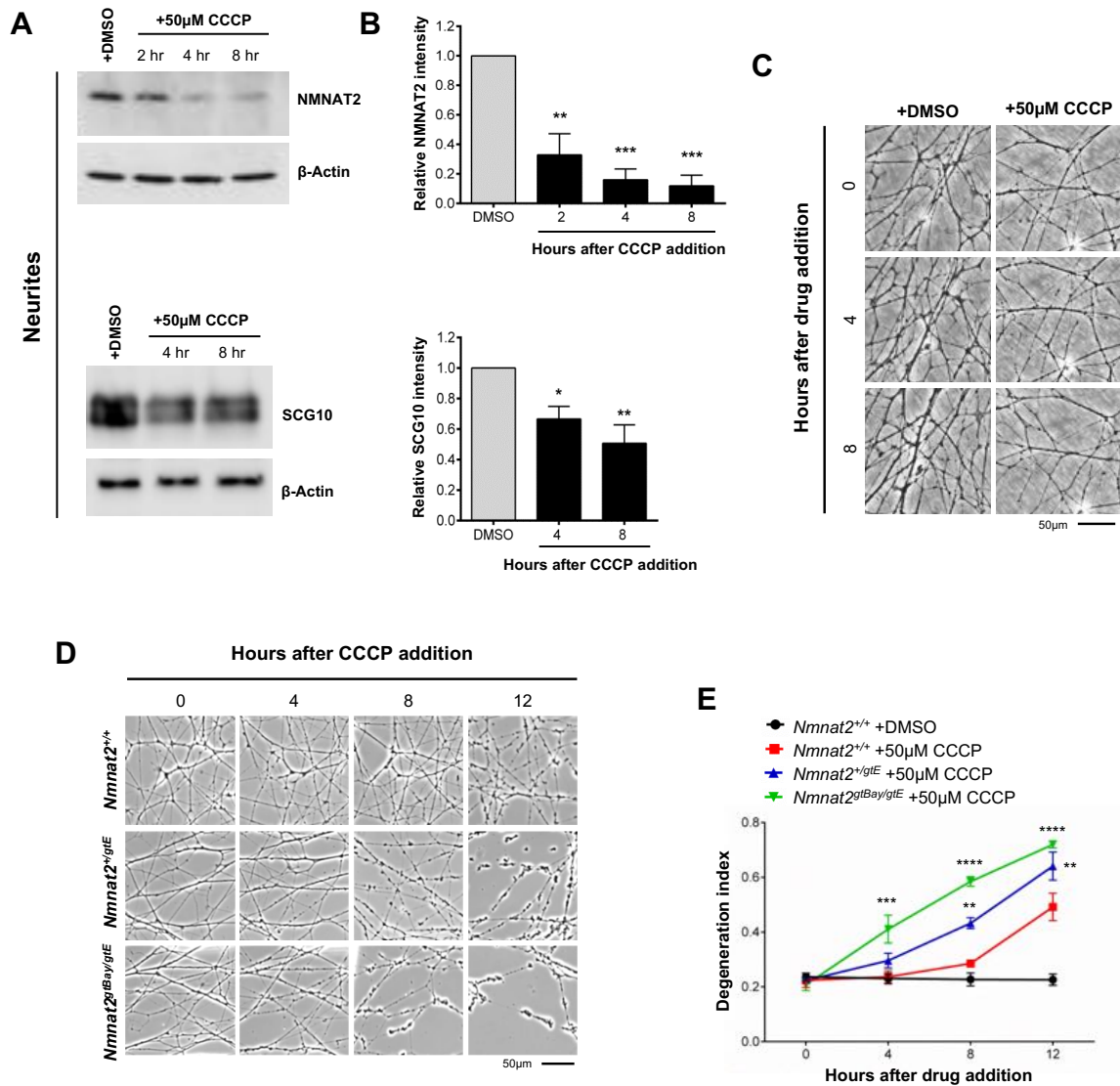
631

632 **Figure 1. Regulators of the Wallerian pathway rescue axon degeneration caused by**
 633 **mitochondrial depolarisation**

634 **(A)** ATP levels in wild-type SCG dissociated cultures after treatment with CCCP. Data are
 635 normalised to DMSO control at each time point (Mean±SEM; n=4; two-way ANOVA followed

636 by Sidak post-hoc test; ****, $p < 0.0001$). **(B)** Representative phase contrast images of neurites
637 from wild-type SCG explant cultures treated with increasing concentrations of CCCP. **(C)**
638 Quantification of the degeneration index in experiments described in (B) from 3 fields per
639 sample in 2 independent experiments (Mean \pm SEM; n=2). **(D)** Representative phase contrast
640 images of neurites from wild-type and *Sarm1*^{-/-} SCG explant cultures at the indicated time
641 points after CCCP treatment. **(E)** Quantification of the degeneration index in experiments
642 described in (D) from 3 fields per sample in 4 independent experiments (Mean \pm SEM; n=4;
643 two-way ANOVA followed by Tukey post-hoc test; ****, $p < 0.0001$. Statistical significance
644 shown relative to +50 μ M CCCP). **(F)** Representative phase contrast images of neurites from
645 wild-type and *Wld*^s SCG explant cultures at the indicated time points after CCCP treatment.
646 **(G)** Quantification of the degeneration index in experiments described in (F) from 3 fields per
647 sample in 4 independent experiments (Mean \pm SEM; n=4; two-way ANOVA followed by Tukey
648 post-hoc test; ****, $p < 0.0001$. Statistical significance shown relative to +50 μ M CCCP).

649

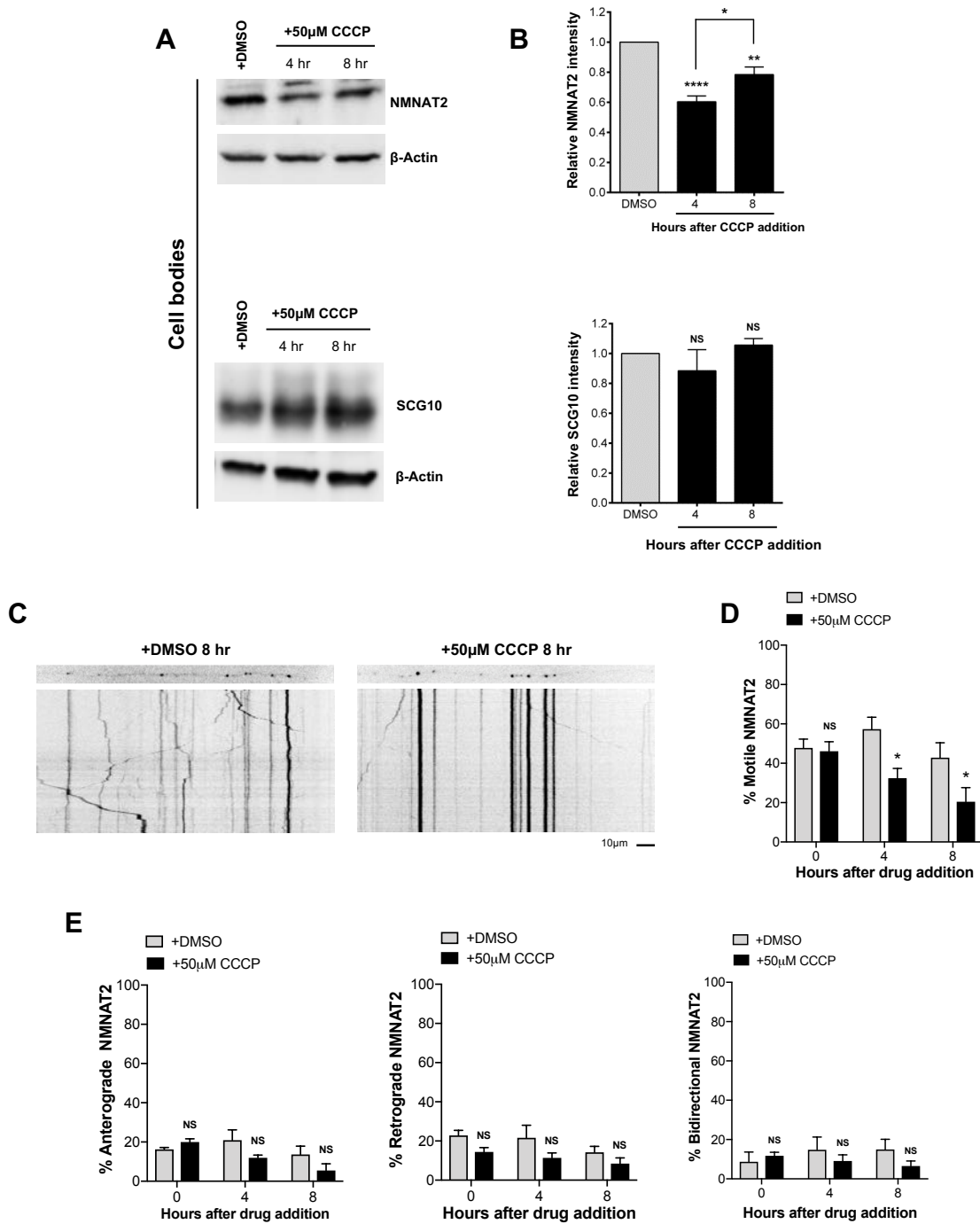


650

651 **Figure 2. Mitochondrial depolarisation leads to depletion of axonal NMNAT2**

652 **(A)** Representative immunoblots of wild-type SCG neurite extracts probed for NMNAT2,
 653 SCG10 and β -actin (loading control) at the indicated time points after CCCP treatment. **(B)**
 654 Quantification of normalised NMNAT2 and SCG10 levels (to β -actin) is shown, with data
 655 presented relative to DMSO control (Mean \pm SEM; n=3-4; one-way ANOVA followed by
 656 Bonferroni post-hoc test; ***, p<0.001; **, p<0.01; *, p<0.05). **(C)** Representative phase
 657 contrast images showing morphologically intact neurites at the time points used in (A). **(D)**
 658 Representative phase contrast images of neurites from wild-type-*Nmnat2*^{+/+}, *Nmnat2*^{+/gtE}
 659 (~60% expression), *Nmnat2*^{gtBay/gtE} (~30% expression) SCG explant cultures at the indicated

660 time points after CCCP treatment. **(E)** Quantification of the degeneration index in experiments
661 described in (D) from 3 fields per sample in 4 independent experiments (Mean±SEM; n=4;
662 two-way ANOVA followed by Tukey post-hoc test; ****, p<0.0001; ***, p<0.001; **, p<0.01.
663 Statistical significance shown relative to *Nmnat2*^{+/+} +50μM CCCP).

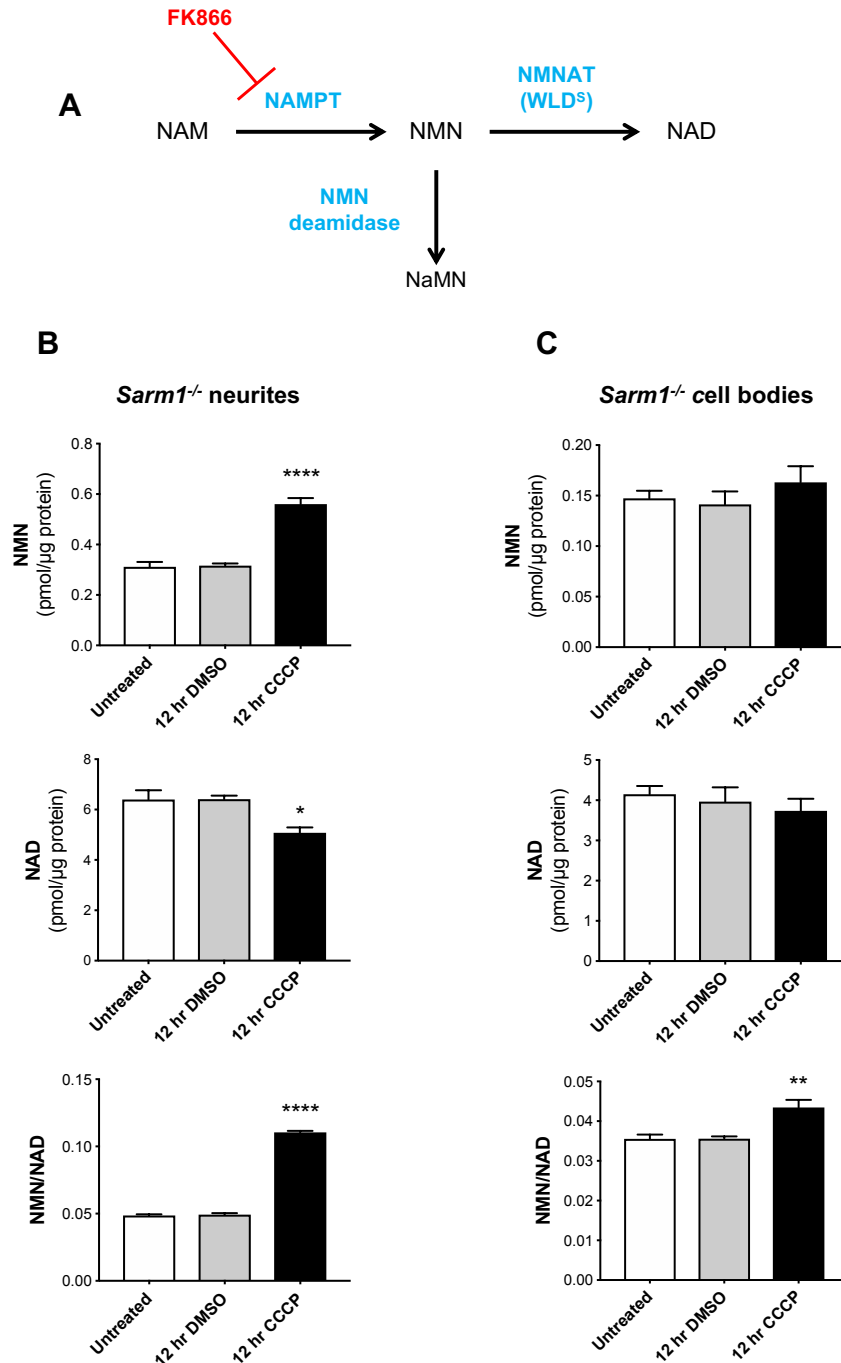


664

665 **Figure 3. NMNAT2 depletion reflects impairment of both axonal transport and synthesis**

666 **(A)** Representative immunoblot of wild-type SCG cell bodies/ganglia extracts probed for
 667 NMNAT2, SCG10 and β -actin (loading control) at the indicated time points after CCCP
 668 treatment. **(B)** Quantification of normalised NMNAT2 and SCG10 levels (to β -actin) is shown,
 669 with data presented relative to DMSO control (Mean \pm SEM; n=4; one-way ANOVA followed by

670 Bonferroni post-hoc test; ****, $p < 0.0001$; **, $p < 0.01$; NS, non-significant). **(C)** Representative
671 kymographs of wild-type SCG dissociated cultures expressing NMNAT2-EGFP. **(D)**
672 Quantification of the % of motile NMNAT2 at the indicated time points after CCCP treatment
673 from 3 neurites per condition in 4 independent experiments (Mean \pm SEM; n=4; two-way
674 ANOVA followed by Sidak post-hoc test; *, $p < 0.05$. NS, non-significant). **(E)** Quantification of
675 the % of motile bidirectional, anterograde and retrograde NMNAT2 at the indicated time points
676 after CCCP treatment from 3 neurites per condition in 4 independent experiments
677 (Mean \pm SEM; n=4; two-way ANOVA followed by Sidak post-hoc test; NS, non-significant).



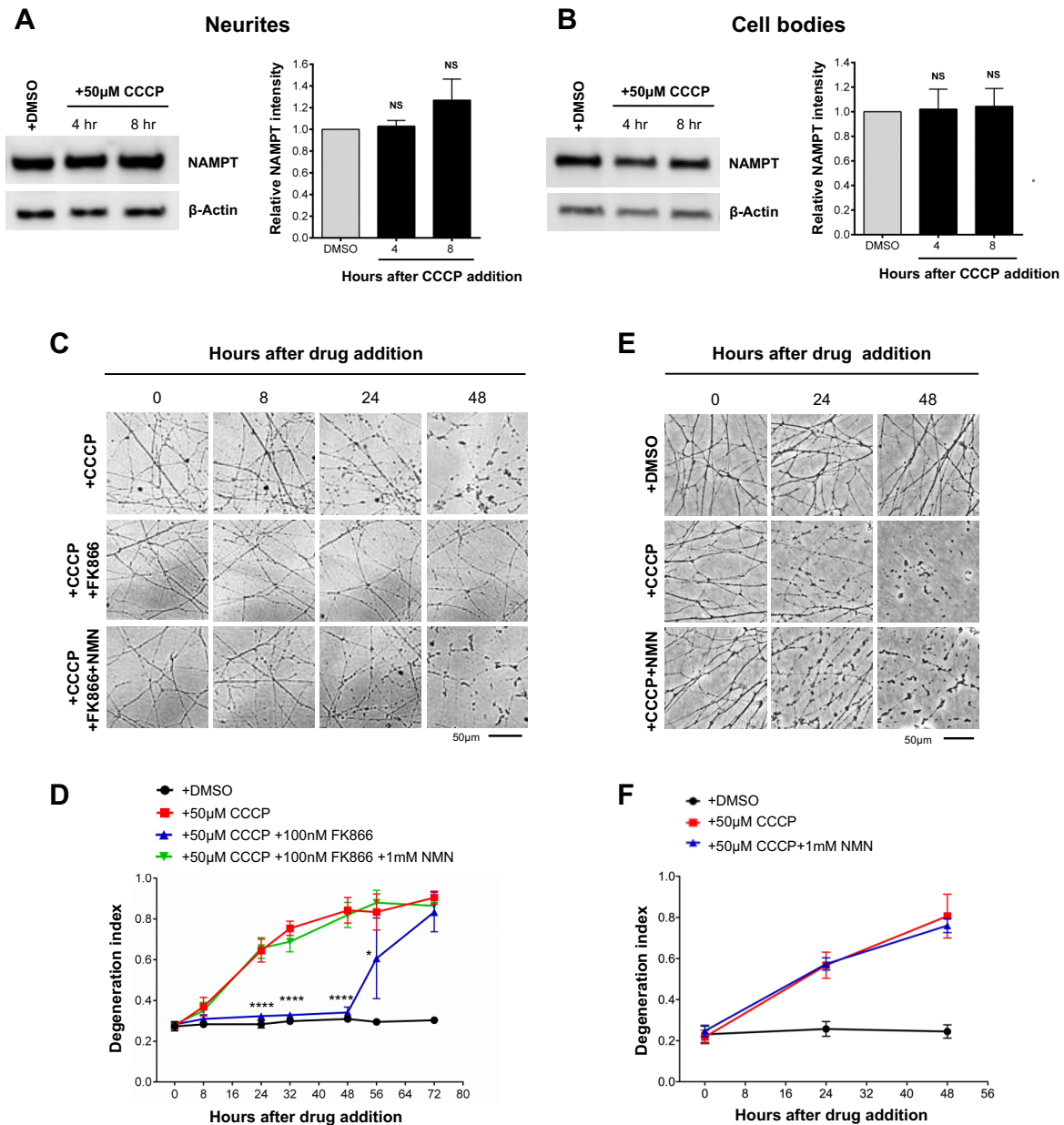
678

679 **Figure 4. Changes in the NMN/NAD ratio following CCCP administration**

680 **(A)** Schematic representation of NAD salvage pathway from nicotinamide and points at which
 681 FK866 and bacterial NMN deamidase will act (NAM, nicotinamide; NaMN, nicotinic acid
 682 mononucleotide; NMN, nicotinamide mononucleotide; NAD, nicotinamide adenine
 683 dinucleotide; NAMPT, nicotinamide phosphoribosyltransferase; NMNAT, nicotinamide
 684 mononucleotide adenylyltransferase). **(B,C)** NMN and NAD levels and NMN/NAD ratios in

685 neurite (B) and cell body/ganglia (C) fractions from *Sarm1*^{-/-} SCG explant cultures at the
686 indicated time points after CCCP treatment (Mean±SEM; n=5; one-way ANOVA followed by
687 Bonferroni post-hoc test; ****, p<0.0001; **, p<0.01; *, p<0.05. Statistical significance shown
688 relative to 12 hr DMSO).

689



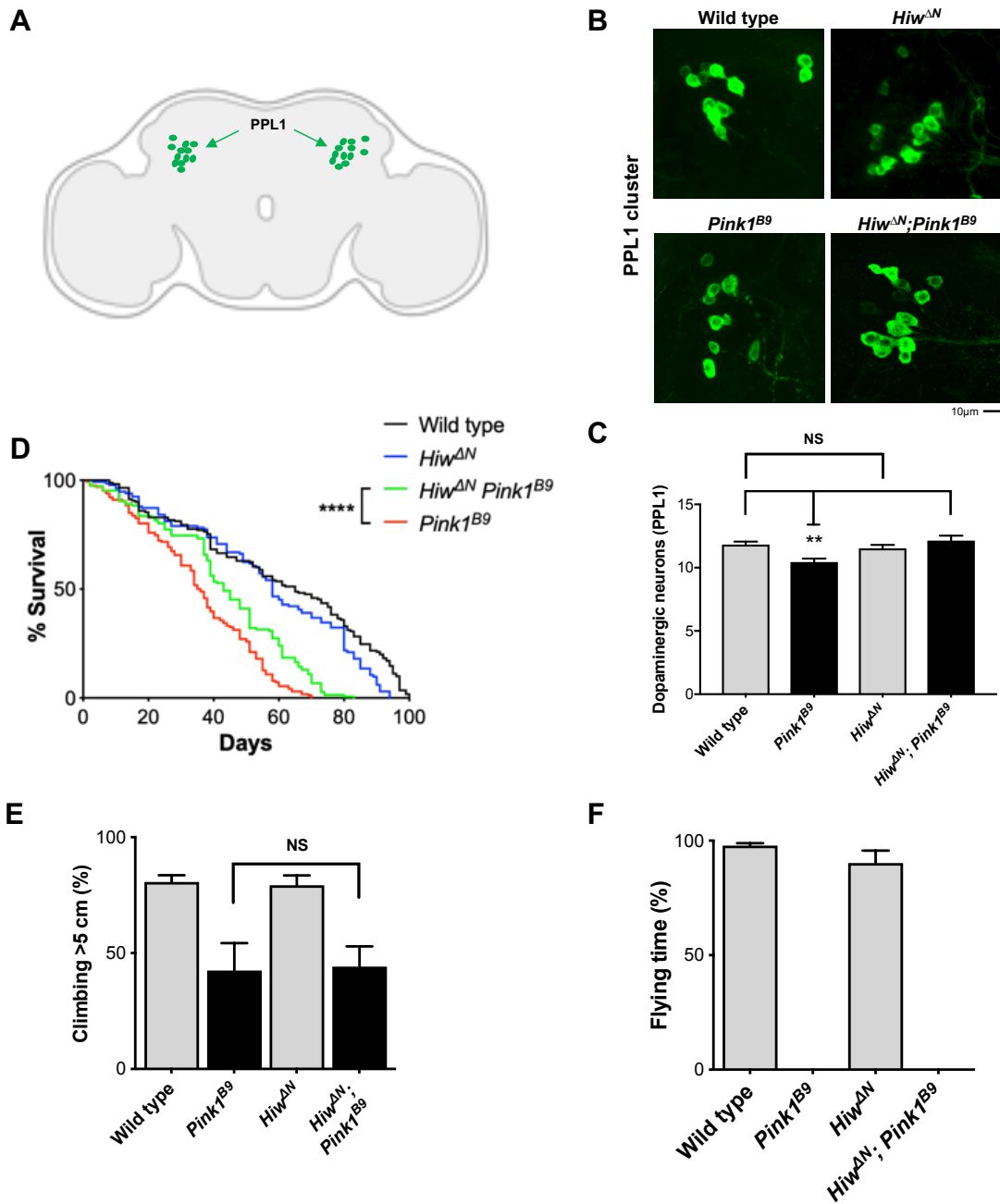
690

691 **Figure 5. Inhibition of NMN synthesis protects neurites against CCCP toxicity**

692 (A,B) Representative immunoblot of wild-type SCG neurite extracts probed for NAMPT and
 693 β -actin (loading control) at the indicated time points after CCCP treatment. Quantification of
 694 normalised NAMPT levels (to β -actin) is shown, with data presented relative to DMSO control
 695 (Mean \pm SEM; n=4; one-way ANOVA followed by Bonferroni post-hoc test; NS, non-significant).
 696 (C) Representative phase contrast images of neurites from wild-type SCG explant cultures at
 697 the indicated time points after CCCP, FK866 and NMN treatment. Where indicated, FK866

698 and NMN were added at the same time of CCCP. **(D)** Quantification of the degeneration index
699 in experiments described in (C) from 3 fields per sample in 4 independent experiments
700 (Mean±SEM; n=4; two-way ANOVA followed by Tukey post-hoc test; ****, p<0.0001.
701 Statistical significance shown relative to +50µM CCCP). **(E)** Representative phase contrast
702 images of neurites from wild-type SCG explant cultures at the indicated time points after CCCP
703 and NMN treatment. **(F)** Quantification of the degeneration index in experiments described in
704 (E) from 3 fields per sample in 4 independent experiments (Mean±SEM; n=4; two-way ANOVA
705 followed by Tukey post-hoc test).

706



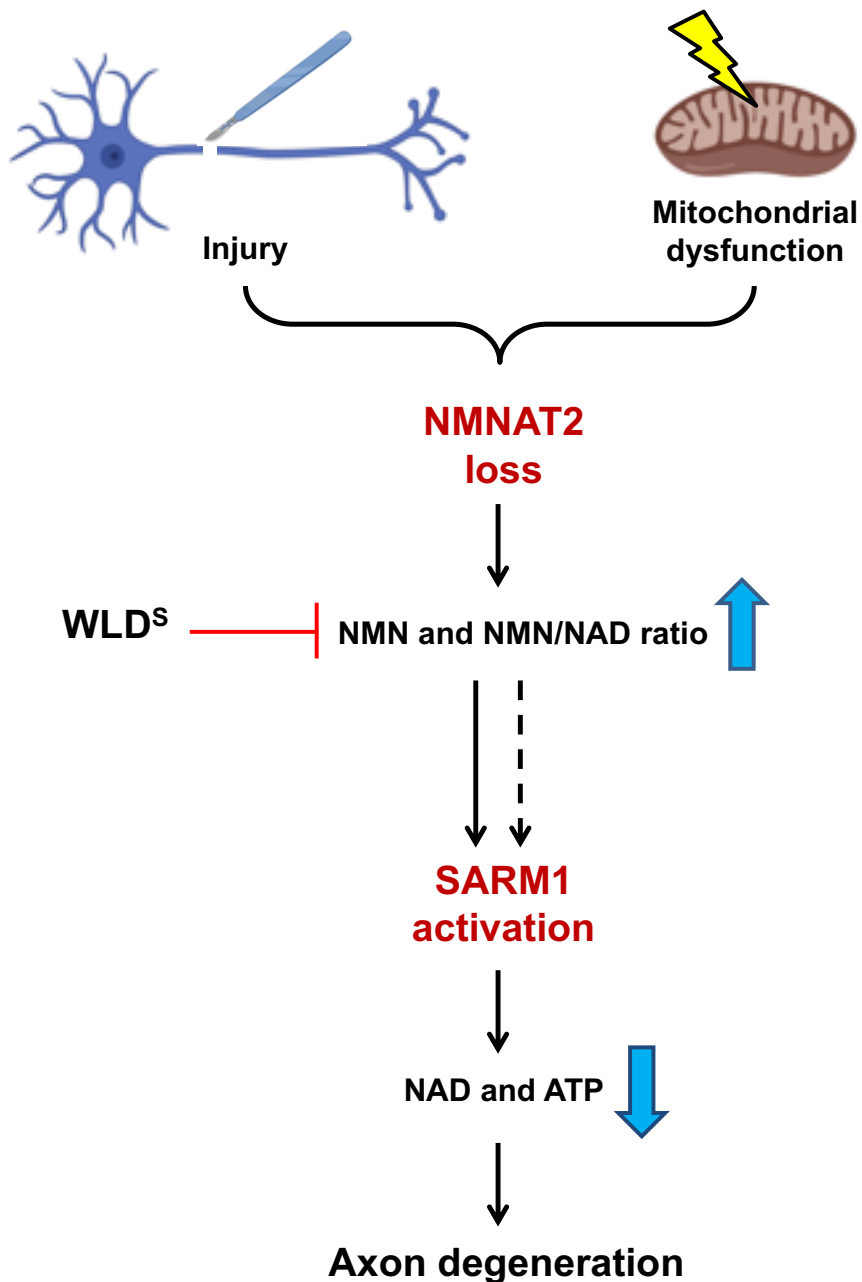
707

708 **Figure 6. Highwire deletion rescues loss of dopaminergic neurons in *Pink1* *Drosophila***
 709 **mutants**

710 **(A)** Schematic image of a *Drosophila* brain with the PPL1 cluster of dopaminergic neurons
 711 shown in green ('Created with BioRender'). **(B)** Representative images of adult *Drosophila* (20
 712 days old) brains stained with anti-TH antibody. The PPL1 cluster of dopaminergic neurons is
 713 shown. **(C)** Quantification of the number of dopaminergic neurons per PPL1 cluster
 714 (Mean±SEM; n=16-25; one-way ANOVA followed by Tukey post-hoc test; **, p<0.01). **(D)**

715 Lifespan curves of wild-type, *Hiw*^{ΔN}, *Pink1*^{B9}, *Hiw*^{ΔN} *Pink1*^{B9} flies (n>130 flies per condition; log-
716 rank (Mantel-Cox) test. ****, p<0.0001). **(E,F)** Analysis of climbing and flying ability of 7 days
717 old flies of the indicated genotypes (Mean±SEM; n=3 climbing, n=9 flying; one-way ANOVA
718 followed by Tukey post-hoc test; NS, non-significant).

719



720

721 **Figure 7. Mitochondrial dysfunction as an upstream signal activating the Wallerian**
722 **pathway**

723 Schematic representation of the Wallerian pathway ('Created with BioRender'). Injury and
724 mitochondrial impairment act as two independent insults resulting in the activation of the
725 Wallerian pathway.